Inorganic Chemistry

Article

pubs.acs.org/IC

Near-Infrared Luminescent PMMA-Supported Metallopolymers Based on Zn−Nd Schiff-Base Complexes

Zhao Zhang,[†] Weixu Feng,[†] Peiyang Su,[†] Xingqiang Lü,*[,†] Jirong Song,[†] Daidi Fan,[†] Wai-Kwok Wong,[‡] Richard A. Jones,[§] and Chengyong Su[⊥]

[†]School of Chemical Engineering, Shaanxi Key Laboratory of Degradable Medical Material, Northwest University, Xi'an 710069, Shaanxi China

[‡]Department of Chemistry, Hong Kong Baptist University, Waterloo Road, Kowloon Tong, Hong Kong, China

[§]Department of Chemistry and Biochemistry, The University of Texas at Austin, 1 University Station A5300, Austin, Texas 78712-0165, United States

[⊥]MOE Laboratory of Bioinoragnic and Synthetic Chemistry/KLGH EI of Environment and Energy Chemistry, School of Chemistry and Chemical Engineering, Sun Yat-Sen University, Guangzhou 510275, Guangdong China

Supporting Information

ABSTRACT: On the basis of self-assembly from the divinylphenyl-modified Salen-type Schiff-base ligands $\mathbf{H_2L^1}$ (*N*,*N*′-bis(5-(3′-vinylphenyl)-3-methoxy-salicylidene)ethylene-1,2-diamine) or $\mathbf{H_2L^2}$ (*N*,*N*′-bis(5-(3′-vinylphenyl)-3-methoxy-salicylidene)-phenylene-1,2-diamine) with $Zn(OAc)_2{\cdot}2H_2O$ and $Ln(NO_3)_3{\cdot}6H_2O$ in the presence of pyridine (Py), two series of heterobinuclear Zn−Ln complexes $[Zn(L'')(Py)Ln(NO_3)_3]$ (*n* = 1, Ln = La, **1**; Ln = Nd, **2**; or Ln = Gd, **3** and *n* = 2, Ln = La, **4**; Ln = Nd, **5**; or Ln = Gd, **6**) are obtained, respectively. Further, through the physical doping and the controlled copolymerization with methyl methacrylate (MMA), two kinds of PMMA-supported hybrid materials, doped **PMMA**/$[Zn(L'')(Py)Ln(NO_3)_3]$ and Wolf Type II Zn^{2+}−Ln^{3+}-containing metallopolymers **Poly(MMA-*co*-**$[Zn(L'')(Py)Ln(NO_3)_3]$**)**, are obtained, respectively. The result of their solid photophysical properties shows the strong and characteristic near-infrared (NIR) luminescent Nd^{3+}-centered emissions for both **PMMA**/$[Zn(L'')(Py)Nd(NO_3)_3]$ and **Poly(MMA-*co*-**$[Zn(L'')(Py)Nd(NO_3)_3]$**)**, where ethylene-linked hybrid materials endow relatively higher intrinsic quantum yields due to the sensitization from both ^{1}LC and ^{3}LC of the chromorphore than those from only ^{1}LC in phenylene-linked hybrid materials, and the concentration self-quenching of Nd^{3+}-based NIR luminescence could be effectively prevented for the copolymerized hybrid materials in comparison with the doped hybrid materials.

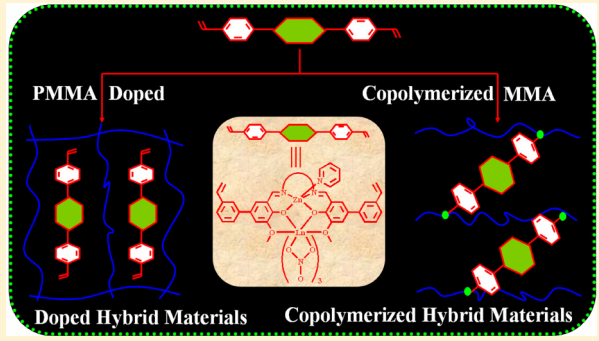

1. INTRODUCTION

Because of the increasing importance on utilization of the near-infrared (NIR) luminescent emission of Nd^{3+} ion in organic light-emitting diodes (OLED),[1] laser materials,[2] telecommunication,[3] and fluoro-immunoassay,[4] there has been a recent interest in synthesizing new kinds of NIR luminescent Nd^{3+} optical materials with those potential applications.[5] From the viewpoint of pursuing excellent photophysical properties for the Nd^{3+} compounds, although many organic ligands[6] and d-block transition metal complexes[7] have been used as antennae or chromophores for the effective sensitization of NIR luminescence of Nd^{3+} ion, it remains a real challenge to enhance NIR quantum efficiency.[8] For this purpose, the energy level's match of the excited state of the chromophore to the Nd^{3+} ion's excited state should be realized[9] besides the complete avoidance or decrease of the luminescent quenching effect arising from OH-, NH-, or CH-oscillators around the Nd^{3+} ions.[10] On the other hand, because of the disadvantage of poor mechanical property and relatively low stability for Nd^{3+} complexes, they were usually applied as the organic−inorganic hybrid materials through physical doping[11] or grafting[12] into stable organic or inorganic matrices. Compared with the difficulty to resolve the high homogeneity and clustering of emitters for those doped hybrid materials with weak interactions between, trapping Nd^{3+} complexes in polymer backbones with covalent bonds should be a good approach to overcome the problem.

Ln^{3+}-containing metallopolymers,[13] as a unique class of grafted hybrid materials, endow the advantage of the beneficial properties of both the characteristic luminescence of Ln^{3+} ions and the attractive features including mechanical strength, flexibility, ease of processing, and low cost of organic polymers. On the basis of the arrangements of Ln^{3+} ions relative to the polymer backbone, three types (Type I, Type II, and Type III)

Received: January 20, 2014
Published: May 28, 2014

   dx.doi.org/10.1021/ic500132n | *Inorg. Chem.* 2014, 53, 5950−5960

described by Wolf have also been realized on the soft metallopolymers,[14] in which the Ln^{3+} metal center is either tethered to the polymeric backbone by a saturated organic linker, covalently coupled to the backbone, or directly incorporated into the polymer backbone, respectively. In contrast to the wide studies on metallopolymers incorporating transition metal ions,[15] the development and application of Ln^{3+}-containing metallopolymers have been relatively limited,[13] which should be due to their synthetic difficulties and lack of effective characterization methods. To the best of our knowledge, the obtained Ln^{3+}-containing metallopolymer systems are usually focused on the mononuclear Ln^{3+} complexes through coupling,[16] ring-opening polymerization,[17] radical polymerization,[18] or electropolymerization,[19] and few systems built from d−f heterometallic complexes,[20] especially no d−f systems with NIR luminescence, are reported.

As a matter of fact, in our or others recent reports, series of ZnLn,[21] Zn_2Ln,[22] Zn_2Ln_2,[23] Zn_2Ln_3,[24] or Zn_4Ln_2 complexes[25] have been obtained from Salen-type Schiff-base ligands, where the 3d Zn^{2+} Schiff-base complexes, as the suitable chromophores, could effectively sensitize the visible or NIR luminescence of the central 4f Ln^{3+} ions. Naturally, by introducing new functions (for example, C═C groups) into 3d Zn^{2+} and 4f Ln^{3+} heterometallic complexes, the polymerizable monomeric complexes may be copolymerized with other C═C-containing monomers, such as methyl methacrylate (MMA), and, thus, new luminescent metallopolymers based on Zn−Ln heterometallic complexes could be expected. Herein, by the self-assembly from the designed divinylphenyl-modified Salen-type Schiff-base ligands $\mathbf{H_2L^1}$ ($\mathbf{H_2L^1}$ = *N*,*N*′-bis(5-(3′-vinylphenyl)-3-methoxy-salicylidene)ethylene-1,2-diamine) and $\mathbf{H_2L^2}$ ($\mathbf{H_2L^2}$ = *N*,*N*′-bis(5-(3′-vinylphenyl)-3-methoxy-salicylidene)phenylene-1,2-diamine) with $Zn(OAc)_2{\cdot}2H_2O$, $Ln(NO_3)_3{\cdot}6H_2O$ (Ln = La, Nd, or Gd), and Py (Py = pyridine), two series of heterobinuclear Zn−Ln complexes $[Zn(L^1)(Py)Ln(NO_3)_3]$ (Ln = La, **1**; Ln = Nd, **2**; or Ln = Gd, **3**) and $[Zn(L^2)(Py)Ln(NO_3)_3]$ (Ln = La, **4**; Ln = Nd, **5**; or Ln = Gd, **6**) are obtained, respectively. The two series of Zn−Ln complex monomers with terminally functional divinylphenyl groups could be copolymerized with MMA; thus, the first example of NIR luminescent Zn−Nd-containing metallopolymers could be expected. The comparison of their photophysical properties with PMMA-based doped hybrid materials is also discussed.

2. EXPERIMENTAL SECTION

2.1. General. High-performance liquid chromatography (HPLC)-grade tetrahydrofuran (THF) was purchased from Fisher Scientific and purified over solvent columns. Other solvents were used as received from Sigma-Aldrich and stored over 3 Å activated molecular sieves. Methyl methacrylate (MMA) was dried over CaH_2, distilled, and stored under dried N_2 prior to use. Azobis(isobutyronitrile) (AIBN) was purified by recrystallization twice from absolute MeOH prior to use. Tetrakis(triphenylphosphine)palladium (0) was synthesized according a well-established literature.[26] Other chemicals were commercial products of reagent grade and were used without further purification. All manipulations of air- and water-sensitive compounds were carried out under dry N_2 using the standard Schlenk line techniques. Elemental analyses were performed on a PerkinElmer 240C elemental analyzer. Infrared spectra were recorded on a Nicolet Nagna-IR 550 spectrophotometer in the region of 4000−400 cm^{-1} using KBr pellets. ^{1}H NMR spectra were recorded on a JEOL EX 400 spectrometer with $SiMe_4$ as internal standard in $CDCl_3$ and/or deuterated dimethyl sulfoxide (DMSO-d_6) at room temperature. Electrospray ionization mass spectrometry (ESI-MS) was performed on a Finnigan LCQ^{DECA} XP HPLC-MS_n mass spectrometer with a mass to charge (m/z) range of 4000 using a standard electrospray ion source and $CHCl_3$ or MeCN as solvent. Electronic absorption spectra in the UV−visible region were recorded with a Cary 300 UV spectrophotometer, steady-state visible fluorescence and PL excitation spectra on a Photon Technology International (PTI) Alpha scan spectrofluorometer, and visible decay spectra were recorded on a pico-N_2 laser system (PTI Time Master). The quantum yield of the visible luminescence for each sample was determined by the relative comparison procedure, using a reference of a known quantum yield (quinine sulfate in dilute H_2SO_4 solution; Φ_{em} = 0.546). NIR emission and excitation spectra in solution or solid state were recorded by PTI QM4 spectrofluorometer with a PTI QM4 Near-Infrared InGaAs detector. Gel permeation chromatography (GPC) analyses of the polymers were performed using a Waters 1525 binary pump coupled to a Waters 2414 refractive index detector with HPLC-grade THF as the eluant on American Polymer Standard 10 μm particle size, linear mixed-bed packing columns. The GPC was calibrated using polystyrene standards. X-ray photoelectron spectroscopy (XPS) was carried out on a PHI 5700 XPS system equipped with a dual Mg X-ray source and monochromatic Al X-ray source complete with depth profile and angle-resolved capabilities. The powder X-ray diffraction (PXRD) patterns were recorded on a D/Max-IIIA diffractometer with graphite-monochromatized Cu Kα radiation (λ = 1.5418 Å). Thermogravimetric (TG) analyses were carried out on a NETZSCH TG 209 instrument under flowing nitrogen by heating the samples from 25 to 600 °C.

2.2. Synthesis of 5-(3′-Vinylphenyl)-3-methoxy-salicylaldehyde. To a solution of 5-bromo-2-hydroxy-3-methoxybenzaldehyde (6.0 g, 26.0 mmol), 3-vinylphenylboronic acid (5.0 g, 33.8 mmol) and tetrakis(triphenylphosphine)palladium (0) (1.1 g) in absolute toluene (100 mL), 30 mL of aqueous 2 M Na_2CO_3 was added, and the resultant mixture was reacted at 80 °C for 24 h. After cooling to room temperature, the solvents were removed by evaporation under reduced pressure, and the residual solid was poured into deionized water (100 mL). The reaction mixture was then extracted with CH_2Cl_2 (3 × 50 mL). The organic layer was dried over anhydrous Na_2SO_4. After evaporation to dryness, the residue was purified by silica column chromatography using a solvent of mixture of *n*-hexane and CH_2Cl_2 (9.5:0.5 v/v) as the eluent to give a pale yellow solid product. Yield: 5.6 g, 84%. Anal. found: C, 75.52; H, 5.62. Calcd for $C_{16}H_{14}O_3$: C, 75.57; H, 5.55%. IR (KBr, cm^{-1}): 3085 (w), 3043 (m), 3010 (m), 2964 (m), 2931 (m), 2854 (m), 1847 (w), 1728 (w), 1649 (s), 1595 (m), 1575 (m), 1473 (vs), 1445 (s), 1421 (m), 1390 (s), 1356 (w), 1331 (s), 1300 (s), 1279 (s), 1265 (s), 1236 (s), 1211 (s), 1177 (m), 1095 (m), 1072 (m), 1049 (w), 997 (m), 960 (s), 921 (m), 895 (m), 864 (w), 827 (w), 808 (m), 785 (s), 750 (s), 731 (s), 715 (vs), 631 (m), 573 (w), 555 (w), 521 (w), 428 (w). ^{1}H NMR (400 MHz, $CDCl_3$): δ (ppm) 11.07 (s, 1H, −OH), 10.00 (s, 1H, −CHO), 7.56 (s, 1H, −Ph), 7.43 (m, 3H, −Ph), 7.39 (d, 1H, −Ph), 7.33 (d, 1H, −Ph), 6.79 (m, 1H, ═CH), 5.83 (d, 1H, ═CH_2), 5.32 (d, 1H, ═CH_2), 4.00 (s, 3H, −OMe). ESI-MS (in $CHCl_3$) m/z: 253.5 (100%), $[M - H]^+$.

2.3. Synthesis of Divinylphenyl-Modified Salen-Type Schiff-Base Ligand H_2L^1 (H_2L^1 = *N*,*N*′-Bis(5-(3′-vinylphenyl)-3-methoxysalicylidene)ethylene-1,2-diamine). To a stirred solution of 1,2-diaminoethane (0.67 mL, 10.0 mmol) in absolute EtOH (50 mL), 5-(3′-vinylphenyl)-3-methoxysalicylaldehyde (5.1 g, 20 mmol) was added, and the resultant mixture was stirred under N_2 atmosphere at room temperature for 24 h. The insoluble yellow precipitate was filtered and washed with cold EtOH and petroleum ether. The crude product was dissolved in $CHCl_3$ (30 mL) and evaporated to dryness to give the yellow polycrystalline solid. Yield: 4.6 g, 86%. Anal. found: C, 76.75; H, 6.09; N, 5.19. Calcd for $C_{34}H_{32}N_2O_4$: C, 76.67; H, 6.06; N, 5.26%. IR (KBr, cm^{-1}): 3238 (b), 3135 (w), 3070 (w), 2972 (w), 2939 (w), 2843 (w), 2808 (w), 1626 (s), 1609 (m), 1599 (w), 1562 (w), 1535 (w), 1520 (m), 1493 (vs), 1460 (s), 1431 (s), 1385 (m), 1348 (w), 1296 (s), 1248 (s), 1204 (m), 1150 (m), 1115 (w), 1053 (m), 1028 (m), 1002 (m), 961 (w), 914 (m), 868 (m), 851 (w), 818 (m), 738 (w), 768 (m), 745 (m), 685 (m), 633 (w), 617 (w), 582 (w), 561 (w), 546 (w), 517 (m), 461 (w), 438 (w), 415 (w). ^{1}H NMR (400 MHz, $CDCl_3$): δ (ppm) 13.71 (s, 2H, −OH), 8.52 (s, 2H, −CH═N), 7.55 (s, 2H, −Ph), 7.40 (m, 6H, −Ph), 7.14 (d, 2H, −Ph), 7.09 (d, 2H, −Ph), 6.79 (m, 2H, ═CH), 5.83

dx.doi.org/10.1021/ic500132n | Inorg. Chem. 2014, 53, 5950−5960

(d, 2H, =CH_2), 5.32 (d, 2H, =CH_2), 4.02 (d, 4H, −CH_2). 3.99 (d, 6H, −OMe).

2.4. Synthesis of [Zn(L^1)(Py)Ln(NO_3)$_3$] (Ln = La, 1; Ln = Nd, 2; Ln = Gd, 3). To a stirred suspension of H_2L^1 (0.160 g, 0.3 mmol) in absolute MeOH (6 mL), $Zn(OAc)_2{\cdot}2H_2O$ (0.066 g, 0.3 mmol) was added, and the resulting mixture was refluxed under N_2 atmosphere for 5 h. A solution of $Ln(NO_3)_3{\cdot}6H_2O$ (0.3 mmol; Ln = La, 0.130 g; Ln = Nd, 0.132 g; or Ln = Gd, 0.135 g) in absolute EtOH (6 mL) and 0.2 mL of pyridine were added. Each resultant respective mixture was stirred under N_2 atmosphere at room temperature for 6 h, and the clear pale yellow solution was filtered. Diethyl ether was allowed to diffuse slowly into the filtrate at room temperature, and the pale yellow microcrystal products of **1**−**3**, respectively, were obtained in a few weeks.

For **1**: Yield: 0.159 g, 53%. Anal. found: C, 46.80; H, 3.55; N, 8.37. Calcd for $C_{39}H_{35}N_6O_{13}ZnLa$: C, 46.84; H, 3.53; N, 8.40%. IR (KBr, cm^{-1}): 3055 (w), 3003 (w), 2981 (w), 2945 (w), 2848 (w), 1637 (s), 1611 (m), 1597 (w), 1556 (m), 1463 (vs), 1394 (s), 1339 (w), 1302 (s), 1267 (vs), 1227 (m), 1215 (m), 1176 (w), 1097 (m), 1070 (w), 1029 (m), 989 (w), 968 (m), 924 (w), 912 (w), 866 (w), 842 (w), 816 (w), 804 (m), 769 (m), 757 (m), 737 (w), 702 (w), 679 (w), 647 (w), 613 (w), 570 (w), 507 (w), 450 (w), 420 (w). ^{1}H NMR (400 MHz, DMSO-d_6−$CDCl_3$ (10:1 v/v)): δ (ppm) 8.71 (s, 1H, −Py), 8.59 (t, 2H, −Py), 8.57 (d, 2H, −CH=N), 7.80 (m, 2H, −Py), 7.71 (s, 1H, −Ph), 7.62 (t, 1H, −Ph), 7.54 (d, 1H, −Ph), 7.49 (d, 2H, −Ph), 7.45 (d, 2H, −Ph), 7.41 (d, 1H, −Ph), 7.39 (m, 2H, −Ph), 7.38 (t, 1H, −Ph), 7.23 (s, 1H, −Ph), 7.18 (d, 1H, −Ph), 6.82 (m, 2H, =CH), 5.95 (m, 2H, =CH_2), 5.33 (m, 2H, =CH_2), 4.12 (s, 3H, −OMe), 4.00 (s, 2H, −CH_2), 3.87 (s, 3H, −OMe), 3.78 (s, 2H, −CH_2). ESI-MS (in MeCN) m/z: 1001.03 (100%), $[M - H]^+$; 938.02 (8%), $[M - NO_3]^+$.

For **2**: Yield: 0.151 g, 50%. Anal. found: C, 46.57; H, 3.58; N, 8.31. Calcd for $C_{39}H_{35}N_6O_{13}ZnNd$: C, 46.59; H, 3.54; N, 8.36. IR (KBr, cm^{-1}): 3057 (w), 3005 (w), 2981 (w), 2947 (w), 2848 (w), 1637 (s), 1610 (m), 1597 (w), 1556 (m), 1463 (vs), 1394 (s), 1339 (w), 1302 (s), 1269 (s), 1226 (m), 1215 (m), 1176 (w), 1097 (m), 1072 (w), 1029 (m), 989 (w), 968 (m), 925 (w), 912 (w), 866 (w), 842 (w), 817 (w), 804 (m), 769 (m), 758 (m), 737 (w), 702 (w), 679 (w), 648 (w), 613 (w), 570 (w), 507 (w), 451 (w), 420 (w). ESI-MS (in MeCN) m/z: 1006.37 (100%), $[M - H]^+$; 943.35 (11%), $[M - NO_3]^+$.

For **3**: Yield: 0.165 g, 54%. Anal. found: C, 45.95; H, 3.49; N, 8.21. Calcd for $C_{39}H_{35}N_6O_{13}ZnGd$: C, 46.00; H, 3.46; N, 8.25. IR (KBr, cm^{-1}): 3058 (w), 3005 (w), 2983 (w), 2946 (w), 2847 (w), 1637 (s), 1610 (m), 1599 (w), 1556 (m), 1461 (vs), 1393 (s), 1339 (w), 1305 (s), 1269 (s), 1225 (m), 1215 (m), 1178 (w), 1097 (m), 1073 (w), 1029 (m), 989 (w), 968 (m), 925 (w), 913 (w), 866 (w), 842 (w), 816 (w), 804 (m), 769 (m), 756 (m), 737 (w), 702 (w), 678 (w), 648 (w), 612 (w), 570 (w), 506 (w), 451 (w), 420 (w). ESI-MS (in MeCN) m/z: 1019.38 (100%), $[M - H]^+$; 956.36 (7%), $[M - NO_3]^+$.

2.5. X-ray Crystallography. Single crystals of [Zn(L^1)(Py)Nd(NO_3)$_3$]·H_2O·MeOH (**2**·H_2O·MeOH) and [Zn(L^2)(Py)Nd(NO_3)$_3$]·0.5H_2O (**5**·0.5H_2O) of suitable dimensions were mounted onto thin glass fibers. All the intensity data were collected on a Bruker SMART CCD diffractometer (Mo Kα radiation and λ = 0.710 73 Å) in Φ and ω scan modes. Structures were solved by direct methods, followed by difference Fourier syntheses, and then refined by full-matrix least-squares techniques against F^2 using SHELXL-97.[27] All other non-hydrogen atoms were refined with anisotropic thermal parameters. Absorption corrections were applied using SADABS.[28] Hydrogen atoms were placed in calculated positions and refined isotropically using a riding model. CCDC reference numbers 971343 and 971344 for **2**·H_2O·MeOH and **5**·0.5H_2O, respectively.

2.6. Synthesis of PMMA Activated with AIBN. The homogeneous polymerization of MMA in activation with AIBN for comparison was carried out in a Fisher−Porter glass reactor and protected by nitrogen according to the typical procedure.[29] To a solution of MMA (2 mL, 19 mmol) in dry 1,2-dichlorobenzene (15 mL), AIBN initiator (46.0 mg, 1.5 mol % of the monomer) was added, and the resultant homogeneous solution was purged with N_2 for 10 min and sealed under a reduced N_2 atmosphere. The mixture was heated to 80 °C with continuous stirring for 24 h. The viscous mixture was diluted with dry 1,2-dichlorobenzene (10 mL) and precipitated with absolute diethyl ether (100 mL) three times. The resulting solid product of PMMA was collected by filtration and dried at 45 °C under vacuum to constant weight. Yield: 91%. IR (KBr, cm^{-1}): 3000 (w), 2951 (m), 2843 (w) 1730 (s), 1631 (m), 1602 (m), 1485 (w), 1454 (w), 1433 (w), 1398 (m), 1384 (m), 1337 (w), 1269 (w), 1238 (w), 1138 (vs), 993 (m), 914 (w), 840 (m), 808 (w), 750 (m), 617 (w), 544 (w), 513 (w), 482 (w). ^{1}H NMR (400 MHz, DMSO-d_6−$CDCl_3$ (10:1 v/v)): δ (ppm) = 3.57 (s, 3H, −COOMe), 1.85 (b, 2H, −CH_2−), 0.91 (m, 3H, −CH_3).

2.7. Synthesis of Doped Hybrid Materials PMMA/[Zn(L^1)(Py)-Ln(NO_3)$_3$] (Ln = La, 1; Ln = Nd, 2; Ln = Gd, 3). A mixture of PMMA obtained from the above homogeneous polymerization of MMA (1 mL, 9.5 mmol) in activation with AIBN (23.0 mg) and [Zn(L^1)Ln(Py)-(NO_3)$_3$] (0.095 mmol; Ln = La (**1**), 95 mg; Ln = Nd (**2**), 96 mg; or Ln = Gd (**3**), 97 mg) was dissolved in dry $CHCl_3$ (20 mL). Each respective mixture was stirred under a reduced N_2 atmosphere at room temperature for 36 h. After each product was precipitated with absolute diethyl ether (100 mL) three times, each resulting solid product was collected by filtration and dried at 45 °C under vacuum to constant weight.

For **PMMA/1** (100:1): Yield: 76%. IR (KBr, cm^{-1}): 3626 (w), 3010 (w), 2947 (w), 2850 (w), 1732 (s), 1636 (m), 1608 (m), 1554 (w), 1464 (vs), 1385 (s), 1304 (s), 1269 (s), 1215 (m), 1176 (w), 1097 (w), 1030 (w), 968 (w), 924 (w), 866 (w), 843 (w), 804 (w), 770 (w), 702 (w), 648 (w), 613 (w), 573 (w), 507 (w). ^{1}H NMR (400 MHz, DMSO-d_6−$CDCl_3$ (v/v = 10:1)): δ (ppm) 8.66 (d, 2H, −CH=N), 8.54 (d, 2H, −Py), 7.73 (t, 1H, −Py), 7.67 (s, 1H, −Ph), 7.61 (s, 1H, −Ph), 7.53 (s, 1H, −Ph), 7.46 (m, 1H, −Py), 7.41 (t, 4H, −Ph), 7.32 (t, 4H, −Ph), 7.12 (m, 2H, −Ph), 6.78 (m, 2H, −CH=C), 5.86 (m, 2H, =CH_2), 5.29 (m, 2H, =CH_2), 4.10 (s, 3H, −OMe), 4.00 (t, 2H, −CH_2), 3.87 (s, 3H, −OMe), 3.75 (t, 2H, −CH_2), 3.55 (s, 182, −COOMe), 1.84 (b, 120, −CH_2−), 0.93 (m, 182, −CH_3).

For **PMMA/2** (50:1, 100:1, or 200:1): Yield: 83% (200:1); 80% (100:1); 75% (50:1). IR (KBr, cm^{-1}): 3624 (w), 3010 (w), 2945 (w), 2850 (w), 1732 (s), 1638 (m), 1604 (m), 1554 (w), 1463 (vs), 1385 (s), 1304 (s), 1269 (s), 1215 (m), 1176 (w), 1095 (w), 1030 (w), 968 (w), 922 (w), 866 (w), 842 (w), 804 (w), 772 (w), 702 (w), 648 (w), 611 (w), 573 (w), 508 (w).

For **PMMA/3** (100:1): Yield: 73%. IR (KBr, cm^{-1}): 3623 (w), 3010 (w), 2945 (w), 2852 (w), 1732 (s), 1638 (m), 1605 (m), 1554 (w), 1464 (vs), 1383 (s), 1304 (s), 1267 (s), 1215 (m), 1174 (w), 1097 (w), 1031 (w), 968 (w), 923 (w), 866 (w), 843 (w), 802 (w), 770 (w), 702 (w), 646 (w), 613 (w), 573 (w), 505 (w).

2.8. Synthesis of Copolymerized Hybrid Materials Poly(MMA-*co*-[Zn(L^1)(Py)Ln(NO_3)$_3$] (Ln = La, 1; Ln = Nd, 2; Ln = Gd, 3). The homogeneous copolymerization of MMA and each of the hetero-binuclear complexes **1**−**3** in activation with AIBN was carried out in a Fisher−Porter glass reactor and protected by nitrogen. To a solution of complexes [Zn(L^1)(Py)Ln(NO_3)$_3$] (0.095 mmol; Ln = La (**1**), 95 mg; Ln = Nd (**2**), 96 mg; or Ln = Gd (**3**), 97 mg) in dry 1,2-dichlorobenzene (15 mL), MMA (9.5 mmol, 1 mL) and AIBN (23.0 mg, 1.5 mol % of MMA) were added, and the resultant homogeneous solution was purged with N_2 for 10 min and sealed under a reduced N_2 atmosphere. The mixture was heated to 80 °C with continuous stirring for 24 h. The viscous mixture was diluted with dry 1,2-dichlorobenzene (10 mL) and precipitated with absolute diethyl ether (100 mL) three times. The respective resulting solid products of **Poly(MMA-*co*-[Zn(L^1)(Py)Ln-(NO_3)$_3$])** were collected by filtration and dried at 45 °C under vacuum to constant weight.

For **Poly(MMA-*co*-1)** (100:1): Yield: 71%. IR (KBr, cm^{-1}): 3630 (w), 3568 (w), 3447 (w), 2995 (w), 2951 (w), 2845 (w), 1732 (vs), 1638 (w), 1616 (w), 1558 (w), 1485 (m), 1450 (m), 1437 (m), 1389 (m), 1270 (m), 1242 (m), 1194 (m), 1148 (vs), 1065 (w), 1036 (w), 988 (m), 966 (m), 912 (w), 843 (w), 810 (w), 750 (m), 710 (w), 650 (w), 617 (w), 482 (w). ^{1}H NMR (400 MHz, DMSO-d_6−$CDCl_3$ (10:1 v/v)): δ (ppm) 8.69 (d, 2H, −CH=N), 8.57 (d, 2H, −Py), 7.77 (t, 1H, −Py), 7.65 (s, 1H, −Py), 7.62 (s, 1H, −Ph), 7.54 (s, 1H, −Py), 7.49 (d, 1H, −Py), 7.45 (d, 2H, −Ph), 7.41 (d, 1H, −Ph), 7.39 (m, 3H, −Ph), 7.28 (m, 2H, −Ph), 7.15 (m, 2H, −Ph), 4.11 (s, 3H, −OMe), 4.00 (s, 2H, −CH_2), 3.86 (s, 3H, −OMe), 3.74 (s, 2H, −CH_2). 3.56 (s, 243H,

dx.doi.org/10.1021/ic500132n | Inorg. Chem. 2014, 53, 5950−5960

−COOMe), 2.92 (m, 2H, −CH), 1.84 (b, 162H, $-CH_2-$), 1.57 (m, 4H, $-CH_2$), 0.93 (m, 243H, $-CH_3$).

For **Poly(MMA-*co*-2)** (50:1, 100:1, or 200:1): Yield: 75% (50:1); 79% (100:1); 81% (200:1). FT-IR (KBr, cm^{-1}): 3632 (w), 3568 (w), 3447 (w), 2993 (w), 2951 (w), 2845 (w), 1731 (vs), 1638 (w), 1616 (w), 1558 (w), 1489 (m), 1450 (m), 1439 (m), 1389 (m), 1271 (m), 1245 (m), 1190 (m), 1146 (s), 1065 (w), 1031 (w), 986 (m), 966 (m), 910 (w), 843 (w), 810 (w), 750 (m), 712 (w), 650 (w), 617 (w), 484 (w).

For **Poly(MMA-*co*-3)** (100:1): Yield: 78%. FT-IR (KBr, cm^{-1}): 3631 (w), 3568 (w), 3445 (w), 2999 (w), 2954 (w), 2843 (w), 1732 (vs), 1638 (w), 1614 (w), 1556 (w), 1485 (m), 1454 (m), 1437 (m), 1389 (m), 1270 (m), 1242 (m), 1194 (m), 1145 (s), 1065 (w), 1034 (w), 988 (m), 966 (m), 910 (w), 843 (w), 811 (w), 750 (m), 711 (w), 650 (w), 619 (w), 482 (w).

3. RESULTS AND DISCUSSION

3.1. Synthesis and Characterization of Two Series of Heterobinuclear Zn−Ln Complexes 1−3 and 4−6. As shown in Scheme 1, the divinylphenyl-modified Salen-type Schiff-base ligand H_2L^1 or H_2L^2 was obtained from the condensation reaction of 1,2-diaminoethane or 1,2-diaminobenzene, respectively, and 5-(3′-vinylphenyl)-3-methoxysalicylaldehyde, which was synthesized by the Suzuki coupling reaction of 3-vinylphenylboronic acid with 5-bromo-2-hydroxy-3-methoxybenzaldehyde. Further, through the reaction of equimolar amounts of the deprotonated Salen-type Schiff-base $(L^1)^{2-}$ or $(L^2)^{2-}$ ligand, $Zn(OAc)_2{\cdot}2H_2O$, and $Ln(NO_3)_3{\cdot}6H_2O$ (Ln = La, Nd, or Gd) in the presence of Py, two series of heterobinuclear Zn−Ln complexes $[Zn(L^1)(Py)Ln(NO_3)_3]$ (Ln = La, **1**; Ln = Nd, **2** and Ln = Gd, **3**) and $[Zn(L^2)(Py)Ln(NO_3)_3]$ (Ln = La, **4**; Ln = Nd, **5**; and Ln = Gd, **6**) were obtained as yellow microcrystalline solids, respectively.

Scheme 1. Reaction Scheme for the Syntheses of Two Divinylphenyl-Modified Salen-Type Schiff-Base Ligands H_2L^1 and H_2L^2 and Two Series of Heterobinuclear Zn−Ln (Ln = La, Nd, or Gd) Complexes 1−3 and 4−6

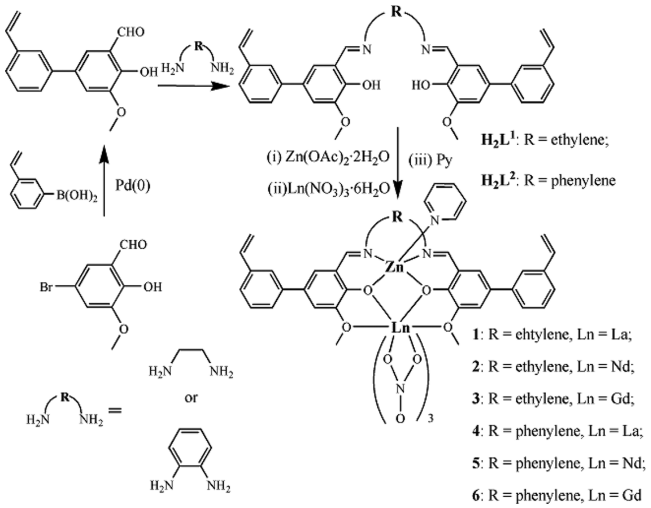

The two divinylphenyl-modified Salen-type Schiff-base ligands H_2L^1, H_2L^2 and the two series of heterobinuclear Zn−Ln (Ln = La, Nd, or Gd) complexes **1**−**3** and **4**−**6** were well-characterized by EA, FT-IR, ^1H NMR, and ESI-MS. In the FT-IR spectra, the characteristic strong absorptions of the ν(C═N) vibration at 1637−1639 cm^{-1} for complexes **1**−**3** or 1652−1660 cm^{-1} for **4**−**6** are slightly blue-shifted by the range of 11−13 or 21−29 cm^{-1} relative to that of the free Salen-type Schiff-base ligand H_2L^1 (1626 cm^{-1}) or H_2L^2 (1631 cm^{-1}) upon the coordination of the Zn^{2+} and Ln^{3+} ions. Moreover, similar to the characteristic absorption of the ν_{as}(C═C) vibration at 1609 or 1614 cm^{-1} for the two terminal vinylphenyl groups of the two ligands H_2L^1 and H_2L^2, the absorptions at 1610−1616 cm^{-1} for complexes **1**−**3** and 1614−1617 cm^{-1} for complexes **4**−**6** are also observed, respectively, which shows that the active terminal vinyl (CH_2═CH−) groups in complexes **1**−**6** are kept upon the coordination of metal ions. For complexes **1**−**6**, two additional strong characteristic absorptions at 1461−1467 and 1301−1305 cm^{-1} for complexes **1**−**3** and 1450−1467 and 1303−1306 cm^{-1} for complexes **4**−**6** were observed, which are tentatively attributed to the ν_{as} vibration and the ν_s vibration of bidentate NO_3^- anions, respectively. As to the room-temperature ^1H NMR spectra of the two Zn−La complexes **1** and **4** shown in Figure 1 and Supporting Information, Figure S1, respectively, besides the disappearance of the typically intramolecular resonance-assisted hydrogen bonded (RAHB) O−H···N proton resonances (vide supra, δ = 13.71 for H_2L^1 or 13.43 ppm for H_2L^2) of the two Salen-type Schiff-base ligands, due to the coordination of the metal ions, slightly spread shifts (δ from 8.71 to 3.78 ppm for **1** and 9.20 to 3.91 ppm for **4**) of the proton resonances of the coordinated ligands for the two complexes in relative to those of the two free ligands (δ from 8.52 to 3.99 ppm for H_2L^1 and 8.69 to 3.92 ppm for H_2L^2) are observed, respectively. The ESI-MS spectra of the two series of complexes **1**−**3** and **4**−**6** in MeCN display the respective similar patterns and exhibit the strong mass peak at *m*/*z* 1001.03 (**1**), 1006.37 (**2**), or 1019.38 (**3**) and 1049.08 (**4**), 1054.41 (**5**), or 1067.42 (**6**) assigned to the major species $\{[Zn(L^1)(Py)Ln(NO_3)_3]-H\}^+$ of complexes **1**−**3** and $\{[Zn(L^2)(Py)Ln(NO_3)_3]-H\}^+$ of complexes **4**−**6**, respectively. These observations further indicate that the respective discrete

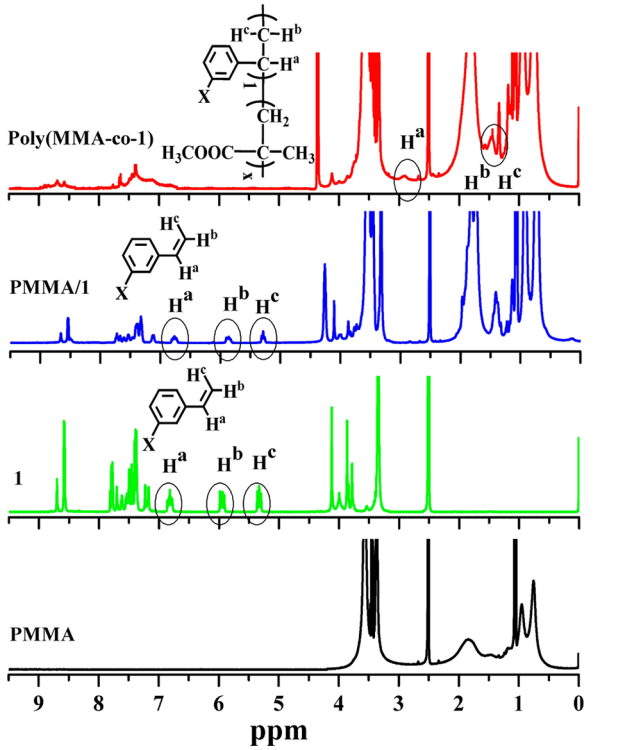

Figure 1. ^1H NMR spectra for PMMA, **1**, **PMMA/1**, and **Poly(MMA-*co*-1)** in DMSO-d_6−$CDCl_3$ (10:1 v/v) at room temperature.

dx.doi.org/10.1021/ic500132n | *Inorg. Chem.* 2014, 53, 5950−5960

heterobinuclear Zn−Ln (Ln = La, Nd, or Gd) unit retains in the respective dilute MeCN solution.

The solid-state structure of **2**·H_2O·MeOH or **5**·0.5H_2O as the respective representative of complexes **1**−**3** and **4**−**6** was determined by single-crystal X-ray diffraction analysis. Crystallographic data for the two complexes are presented in Table 1, and

Table 1. Crystal Data and Structure Refinement for Complexes 2·H_2O·MeOH and 5·0.5H_2O

compound	2·H_2O·MeOH	5·0.5H_2O
formula	$C_{40}H_{41}N_6O_{15}ZnNd$	$C_{43}H_{36}N_6O_{13.5}ZnNd$
fw	1055.40	1062.39
size, mm	0.33 × 0.28 × 0.20	0.31 × 0.27 × 0.23
T, K	296(2)	296(2)
cryst syst	monoclinic	monoclinic
space group	$P2_1$	$P2_1(n)$
a, Å	12.009(3)	12.3057(12)
b, Å	15.962(3)	14.6933(14)
c, Å	13.365(3)	24.791(2)
α, deg	90	90
β, deg	112.938(4)	90.430(2)
γ, deg	90	90
V, Å^3	2359.3(9)	4482.4(7)
Z	2	4
ρ, g cm^{-3}	1.486	1.574
μ, mm^{-1}	1.666	1.752
F(000)	1066	2136
data/restraints/parameters	7900/1068/551	9326/1087/586
quality-of-fit indicator	1.047	1.107
final R indices [$I > 2\sigma(I)$]	R_1 = 0.0806	R_1 = 0.0796
	$_wR_2$ = 0.1861	$_wR_2$ = 0.2189
R indices (all data)	R_1 = 0.1374	R_1 = 0.1517
	$_wR_2$ = 0.2294	$_wR_2$ = 0.2583

selected bond lengths and angles are given in Supporting Information, Table S1. Complex **2**·H_2O·MeOH crystallizes in the monoclinic space group $P2_1$. For complex **2**·H_2O·MeOH, the structural unit is composed of one neutral [Zn(L^1)(Py)Nd-$(NO_3)_3$] part, one solvate H_2O, and one solvate MeOH. As shown in Figure 2, for the [Zn(L^1)(Py)Nd$(NO_3)_3$] part, the relatively soft Zn^{2+} (Zn1) ion in the inner *cis*-N_2O_2 core and the hard Nd^{3+} (Nd1) ion in the outer O_2O_2 moiety of the vinylphenyl-modified Salen-type Schiff-base ligand $(\mathbf{L^1})^{2-}$ are bridged by two μ-O phenoxide atoms (O2 and O3) of the ligand $(\mathbf{L^1})^{2-}$, resulting in the formation of the typical heterobinuclear host structure. The Zn^{2+} (Zn1) ion has a common five-

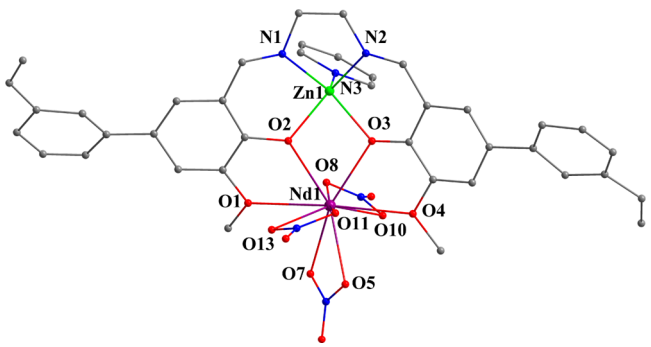

Figure 2. Perspective drawing of the host heterobinuclear structure in **2**·H_2O·MeOH; H atoms and solvates are omitted for clarity.

coordinate environment and adopts a distorted square pyramidal geometry, as shown by the τ value of 0.185, composed of the inner *cis*-N_2O_2 core from the ligand $(\mathbf{L^1})^{2-}$ as the base plane and one N (N3) atom from the coordinated Py at the apical position. As to the Nd^{3+} (Nd1) ion, it is 10-coordinate: in addition to four O atoms from the outer O_2O_2 moiety of the ligand $(\mathbf{L^1})^{2-}$, another six O atoms are contributed from three bidentate NO_3^- anions. The 10 Nd−O bond lengths (2.398(8)−2.710(8) Å) depend on the nature of the O atoms, where the bond lengths from six O atoms of three NO_3^- anions (2.490(10)−2.597(10) Å) are shorter than those (2.652(8)−2.710(8) Å) from two O atoms (O1 and O4) of two −OMe groups while longer than those (2.398(8)−2.453(8) Å) from two phenoxide O atoms. The solvates MeOH and H_2O molecules of complex **2**·MeOH·H_2O are not bound to the framework, and they also exhibit no observed interactions with the host structure.

The change of linker group from ethylene to phenylene ($\mathbf{H_2L^1}$ to $\mathbf{H_2L^2}$) does not lead to a significant change of the host heterobinuclear structure of complex **5**·0.5H_2O shown in Supporting Information, Figure S2, while it endows the extended conjugation with relatively shorter Zn···Nd separation of 3.510(2) Å than that (3.553(2) Å) in complex **2**·H_2O·MeOH. It is worth noting that although the comparable axial occupations of the Zn^{2+} ion from neutral Py in the two complexes to those from Py or bipyridyl in heterobinuclear,[21b] heterotrinuclear,[22a] or heterotetranuclear complexes[23a] based on typical Salen-type Schiff-base ligands with the outer O_2O_2 moiety or not are observed, from which it effectively avoids the further coordination of oscillators-containing bridges or solvates around the Nd^{3+} ions, the introduction of two functional terminal vinylphenyl groups (with the typical C═C bond lengths of 1.315(17)−1.332(15) Å with the trans mode in **2**·H_2O·MeOH or 1.246(16)−1.309(15) Å with the cis mode in **5**·0.5H_2O for the vinyl groups) in the two complexes should be active in the following copolymerization.

3.2. Photophysical Properties of Two Series of Heterobinuclear Zn−Ln Complexes 2−3 and 5−6 in Solution. The photophysical properties of ligands $\mathbf{H_2L^1}$ and $\mathbf{H_2L^2}$ and complexes **2**−**3** and **5**−**6** were examined in dilute MeCN solution at room temperature or 77 K and summarized in Table 2, Figures 3 and 4, and Supporting Information, Figure S3. As shown in Figure 3, similar ligand-centered solution absorption spectra of complexes **2** and **3** (256 and 356−357 nm) in the UV−visible region are observed, respectively, red-shifted upon coordination to metal ions as compared to that (248 and 330 nm) of the free divinylphenyl-modified Salen-type Schiff-base ligand $\mathbf{H_2L^1}$. For complex **2**, very weak visible emission (λ_{em} = 501 nm, τ < 1.0 ns, and $\phi_{em} < 10^{-5}$) is observed in dilute MeCN solution at room temperature, which can be assigned to the $\pi-\pi^*$ transition of the ligand. In addition to the weak residual visible emission, as shown in Figure 4, photoexcitation of the antenna in the range of 250−450 nm (λ_{ex} = 370 nm) gives rise to the characteristic ligand-field splitting emissions of the Nd^{3+} ion ($^4F_{3/2} \rightarrow {}^4I_{J/2}$, J = 9, 11, 13) in the NIR range, respectively, where the emissions at 907, 1064, and 1324 nm can be assigned to $^4F_{3/2} \rightarrow {}^4I_{9/2}$, $^4F_{3/2} \rightarrow {}^4I_{11/2}$, and $^4F_{3/2} \rightarrow {}^4I_{13/2}$ transitions of the Nd^{3+} ion, respectively. The free ligand $\mathbf{H_2L^1}$ and its Zn−Gd complex **3** do not exhibit NIR luminescence under the same conditions, but they do display the typical strong luminescent emissions (shown in Supporting Information, Figure S3) of the Schiff-base ligand in the visible region. Moreover, for complex **2**, the excitation spectrum monitored at the "hypersensitive" NIR emission peak (λ_{em} = 1064 nm) is similar to that monitored at the weak residual

dx.doi.org/10.1021/ic500132n | Inorg. Chem. 2014, 53, 5950−5960

Table 2. Photophysical Properties of Ligands H_2L^1 and H_2L^2 and Complexes 2−3 and 5−6 at 1×10^{-5} M in Absolute MeCN Solution or Solid State, PMMA/$[Zn(L^n)(Py)Ln(NO_3)_3]$ and Poly(MMA-*co*-$[Zn(L^n)(Py)Ln(NO_3)_3]$) (n = 1 or 2; Ln = Nd or Gd) in Solid State at Room Temperature or 77 K

	absorption	excitation	emission
compound	λ_{ab}, nm [log(ε, dm^3 mol^{-1} cm^{-1})]	λ_{ex}, nm	λ_{em}, nm (τ, $\Phi \times 10^3$)
H_2L^1	248 (0.43), 330 (0.06)	309	384 (s, 1.36 ns, 0.47)
2[a]	256 (1.16), 356 (0.09)	316 (sh), 370	501 (w, <1 ns, <10^{-2}); 907 (sp), 1064 (2.81 μs), 1324
2[b]	282, 370, 580, 742, 800, 874	393	503 (<1 ns), 906 (sp), 1062 (2.76 μs), 1326
3[a]	256 (1.13), 357 (0.13)	313, 373	502 (m, 1.14 ns, 0.024) 495 (s, 2.26 ns, 77 K), 548 (5.78 ms, 77 K)
3[b]	283, 372	393	505 (m, 1.12, 0.018) 4.93 (s, 2.12 ns, 77 K), 534 (7.8 ms, 77 K)
H_2L^2	250 (0.30), 283 (0.20), 336 (0.09)	350	508 (1.81 ns, 0.72)
5[a]	256 (0.61), 288 (0.63), 344 (0.28), 406 (0.09)	358, 412 (sh)	536 (m, 1.22 ns, 0.012), 908 (sp), 1067 (1.67 μs), 1340
5[b]	292, 354, 412, 582, 738, 798, 870	414	904 (sp), 1066 (1.62 μs), 1332
6[a]	256 (0.65), 288 (0.68), 346 (0.31), 408 (0.12)	361, 403	534 (s, 5.42 ns, 0.066) 521 (s, 9.14 ns, 77K)
6[b]	293, 353, 413	410	541 (s, 4.56 ns, 0.068) 529 (s, 7.57 ns, 77 K)
PMMA/2	282, 370, 580, 740, 800, 872	398	496 (<1 ns, <10^{-2}), 882 (sp), 1066 (2.72 μs), 1322
PMMA/3	283, 370	323 (sh), 371	498 (m, 1.17 ns, 0.009) 492 (2.10 ns, 77 K), 532 (8.2 ms, 77 K)
PMMA/5	291, 352, 412, 581, 740, 802, 870	418	535 (m, 1.13 ns, 0.014), 878 (sp), 1062 (1.65 μs), 1328
PMMA/6	292, 370, 412	355, 405 (sh)	538 (s, 4.65 ns, 0.074) 525(s, 7.82 ns, 77 K)
Poly(MMA-*co*-2)	296, 376, 582, 740, 798, 870	394	513(vw, <1 ns, <10^{-2}), 882(sp), 1066(3.01 μs), 1324
Poly(MMA-*co*-3)	295, 374	331(sh), 375	510(w, 0.82 ns, 0.73) 504 (2.41 ns, 77 K), 567 (12.3 ms, 77 K)
Poly(MMA-*co*-5)	302, 356, 418, 582, 742, 800, 870	412	554 (w, 0.74 ns, 0.057), 881 (sp), 1066 (1.89 μs), 1334
Poly(MMA-*co*-6)	300, 358, 416	356, 414 (sh)	558 (m, 7.85 ns, 0.057) 545 (s, 14.52 ns, 77K)

[a]In absolute MeCN solution. [b]In solid state.

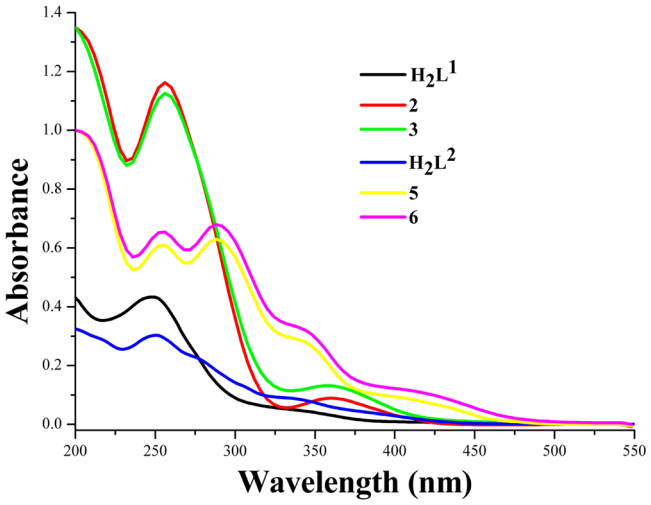

Figure 3. UV−visible absorption spectra of the ligands H_2L^1 and H_2L^2 and complexes **2**−**3** and **5**−**6** in absolute MeCN solution at 1×10^{-5} M at room temperature.

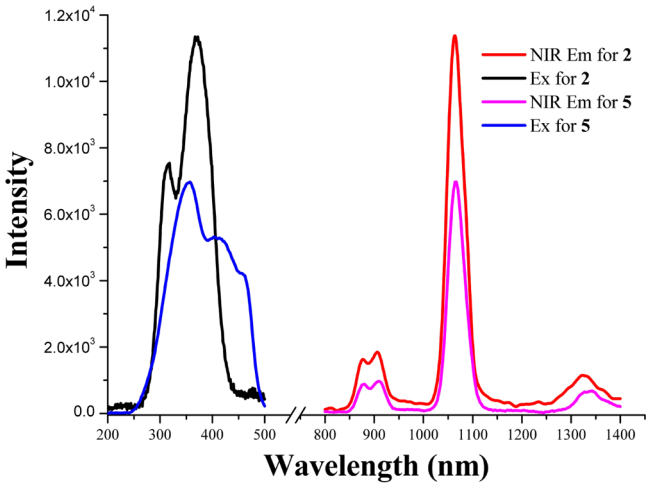

Figure 4. NIR emission and excitation spectra of complexes **2** and **5** in absolute MeCN solution at 1×10^{-5} M at room temperature.

visible emission peak (λ_{em} = 501 nm), which demonstrates that both the NIR and visible emissions are originated from the same the $\pi-\pi^*$ transitions of the Schiff-base ligand of H_2L^1. This, together with the distinctive decrease of visible emission of complex **2** relative to its Zn−Gd complex **3**, suggests that the energy transfer from the antenna to Nd^{3+} ion takes place efficiently in complex **2**.[30] Further, on the basis of the time-resolved luminescent experiment for NIR luminescent complex **2**, the luminescent decay curve can be fitted monoexponentially with lifetime of 2.81 μs, indicating the presence of only one emissive Nd^{3+} ion center. The intrinsic quantum yield (1.12%) of the Nd^{3+} ion emission for complex **2** may be estimated by $\phi_{Nd} = \tau_{obs}/\tau_0$,[31] where τ_{obs} is the observed emission lifetime and τ_0 is the "neutral lifetime" of 0.25 ms for the Nd^{3+} ion. As the suitable reference compound, the Zn−Gd complex **3** allows the study of the antenna luminescence in the absence of energy transfer,

dx.doi.org/10.1021/ic500132n | Inorg. Chem. 2014, 53, 5950−5960

Scheme 2. Reaction Scheme for the Synthesis of Doped Hybrid Materials PMMA/[Zn(L^n)(Py)Ln(NO$_3$)$_3$] and Copolymerized Hybrid Materials Poly(MMA-*co*-[Zn(L^n)(Py)Ln(NO$_3$)$_3$]) (n = 1 or 2, Ln = La, Nd, or Gd)

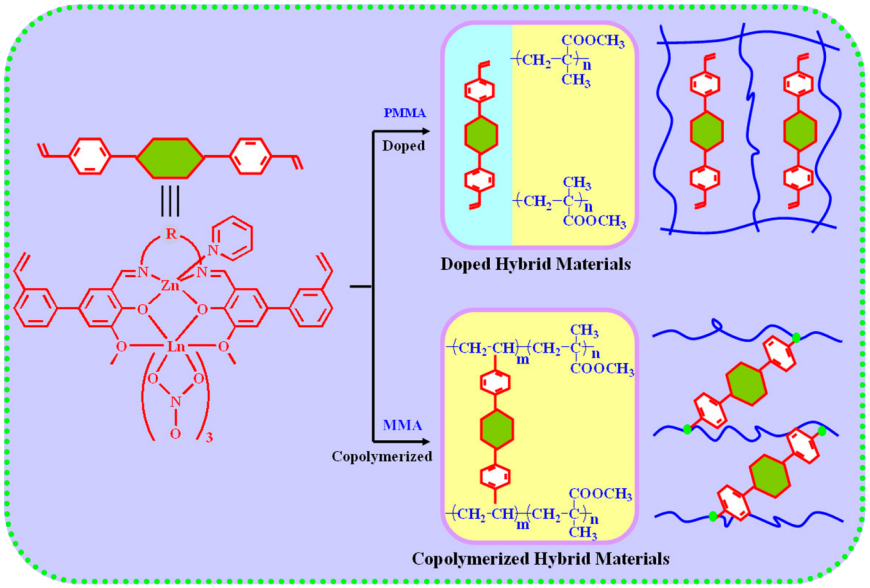

because the Gd^{3+} ion has no energy levels below 32 150 cm^{-1} and, therefore, cannot accept any energy from the corresponding antenna excited state.[32] If the antenna luminescence lifetime of complex **3** is to represent the excited-state lifetime in the absence of the energy transfer, the energy transfer rate (k_{ET}) in complex **3** can, thus, be calculated from $k_{ET} = 1/\tau_q - 1/\tau_u$,[33] where τ_q is the residual lifetime of the luminescent emission undergoing quenching by the respective Nd^{3+} ion, and τ_u is the unquenched lifetime in the reference complex **3**, so the energy transfer rate for the Nd^{3+} ion in complex **2** may be estimated to be above 1.2 × 10^8 s^{-1}, which could well imply the reason for the effective energy transfer for complex **2**. Through further investigation on the emission of the reference complex **3**, especially at 77 K, the stronger fluorescence (λ_{em} = 495 nm and τ = 2.26 ns) than that (λ_{em} = 502 nm and τ = 1.14 ns) at room temperature and the typical phosphorescence (λ_{em} = 548 nm and τ = 5.78 ms) are both observed, which shows that the sensitization of the NIR luminescence in complex **2** should arise from both the ^{1}LC and the ^{3}LC excited states (Supporting Information, Figure S4) of the ligand $\mathbf{H_2L^1}$ at low temperature.

By extension of the conjugation through changing the linker from ethylene to phenylene ($\mathbf{H_2L^1}$ to $\mathbf{H_2L^2}$), the similar photophysical properties, also shown in Table 2, Figures 3 and 4, and Supporting Information, Figure S3, are observed. The typical decay profile for NIR luminescent complex **5** also reveals the single exponential function with the observed lifetime of 1.67 μs and the estimated intrinsic quantum yield of 0.67%. As to the phenylene-linked Zn−Gd complex **6** from $\mathbf{H_2L^2}$, time-resolved spectra show that the visible emissions at both room temperature and 77 K correspond to ^{1}LC emission with lifetimes of 5.42 and 9.14 ns, respectively. The relatively larger energy gap between the only ^{1}LC but no ^{3}LC for complex **5** (Supporting Information, Figure S4, ΔE^1 = 7937 cm^{-1}) than that (ΔE^3 = 6991 cm^{-1}) of both ^{3}LC and ^{1}LC for complex **2** and the excited state $^4F_{3/2}$ (11257 cm^{-1}) of Nd^{3+} ion, should be attributed to the relatively higher estimated intrinsic quantum yield of complex **2** than that of complex **5**.[22a] Moreover, when comparing the relative intensities, using solutions with their concentrations adjusted to give the same absorbance values at 337 nm, the 1.6 times greater emission intensity of complex **2** at 1060 nm relative to that of complex **5** further indicates more efficient energy transfer for ethylene-linked complex **2**.

3.3. Synthesis and Characterization of Doped Hybrid Materials PMMA/[Zn(L^n)Ln(Py)(NO$_3$)$_3$] and Copolymerized Hybrid Materials Poly(MMA-*co*-[Zn(L^n)Ln(Py)(NO$_3$)$_3$]). In consideration of the excellent performance of PMMA as one of the popular polymer matrices with low cost, low optical absorbance, and good mechanical property,[34] two kinds of PMMA-supported doped hybrid materials **PMMA/[Zn(L^n)Ln(Py)(NO$_3$)$_3$]** (n = 1−2, Ln = La, Nd, or Gd) and copolymerized hybrid materials **Poly(MMA-*co*-[Zn(L^n)Ln(Py)(NO$_3$)$_3$])** are obtained from complexes **1**−**6**, respectively, as shown in Scheme 2. The doped hybrid materials **PMMA/[Zn(L^n)Ln(Py)(NO$_3$)$_3$]** based on complexes **1**−**3** and **4**−**6** are well-verified by FT-IR spectra, where the characteristic absorptions of the ν_{as}(C═C) vibration of vinyl groups at 1604−1616 cm^{-1} for complexes **1**−**6** and the characteristic absorptions of the ν(C═N) vibration at 1636−1638 cm^{-1} for complexes **1**−**3** or 1650−1651 cm^{-1} for complexes **4**−**6** are well kept, and the intense absorption band at 1732 or 1737 cm^{-1} assigned to the ν(C═O) vibration of PMMA appears. Especially based on the room-temperature ^{1}H NMR spectra of two hybrid materials **PMMA/1** (shown in Figure 1) and **PMMA/4** (shown in Supporting Information, Figure S1), the combination of almost no shifted proton resonances of the coordinated Salen-type Schiff-base ligand $(\mathbf{L^1})^{2-}$ or $(\mathbf{L^2})^{2-}$ in comparison with those of the respective complex **1** or **4** and the appearance of typical proton resonances of PMMA are observed. Both indicate that two series of heterobinuclear Zn−Ln complexes (**1**−**6**) are just being physically doped into the PMMA polymer matrices. It is worth noting that for the doped hybrid material **PMMA/1** or **PMMA/4**, ^{1}H NMR analysis (Figure 1 and Supporting Information, Figure S1) further shows the lower molar ratio of 60:1 or 75:1 than the initial feed molar ratio of 100:1, which should be due to the loss of MMA from polymerization incompleteness and oligomeric PMMA.

In contrast to the doping, two series of binuclear Zn−Ln complexes (**1**−**6**) with two active terminal vinyl groups can be

dx.doi.org/10.1021/ic500132n | Inorg. Chem. 2014, 53, 5950−5960

further copolymerized with MMA in the presence of AIBN through the classic free-radical mechanism, resulting in the obtainment of the copolymerized hybrid materials **Poly(MMA-*co*-[Zn(L″)Ln(Py)(NO$_3$)$_3$])**. As expected, each of the Zn−Ln units is coupled to the polymer backbone; thus, the only Wolf Type II metallopolymers based on the heterobinuclear units are constructed to date. The obtained metallopolymers with Wolf Type II fashion are also well-characterized by FT-IR and ^{1}H NMR. As to **Poly(MMA-*co*-1)** or **Poly(MMA-*co*-4)** based on Zn−La unit, the ^{1}H NMR spectrum analysis (shown in Figure 1 or Supporting Information, Figure S1) shows that the combined photon resonances (δ = 8.69 to 0.93 ppm for **Poly(MMA-*co*-1)** or δ = 9.20 to 0.94 ppm for **Poly(MMA-*co*-4)**) of the polymerized Schiff-base ligand and MMA are observed, where the photon resonances of the characteristic vinyl groups disappears, while the new up-shifted photon resonances (δ = 2.92 and 1.57 ppm or 2.95 and 1.57 ppm) of the −CH and −CH$_2$ groups are observed, and the lower molar ratio of 81:1 or 61:1 than the initial feed molar ratio of 100:1 is also shown. The relatively higher molar ratio of 81:1 for **Poly(MMA-*co*-1)** should be due to the flexibility of ethylene linker in complex **1**, but it proves that the copolymerization is more complete than that from complex **4**. As shown in Table 3, the GPC results show that

Table 3. GPC Data of the Samples of PMMA and Metallopolymers Poly(MMA-*co*-[Zn(L″)(Py)Ln(NO$_3$)$_3$]

sample	monomer	MMA/monomer	M_n[a] g·mol	PDI[b]
PMMA	MMA		45 255	1.15
Poly(MMA-*co*-1)	MMA and **1**	100:1	11 904	1.21
Poly(MMA-*co*-2)	MMA and **2**	50:1	7149	1.30
Poly(MMA-*co*-2)	MMA and **2**	100:1	11 829	1.23
Poly(MMA-*co*-2)	MMA and **2**	200:1	13 824	1.19
Poly(MMA-*co*-3)	MMA and **3**	100:1	11 630	1.24
Poly(MMA-*co*-4)	MMA and **4**	100:1	9229	1.28
Poly(MMA-*co*-5)	MMA and **5**	100:1	8130	1.26
Poly(MMA-*co*-6)	MMA and **6**	100:1	9145	1.27

[a] M_n is the number molecular weight. [b] PDI = M_w/M_n, where M_w is the weight molecular weight.

all the polydispersity indexes (PDI = M_w/M_n) of these metallopolymers are in the relatively narrow range of 1.19−1.30 due to the radical copolymerization as compared to homopolymerization of MMA using AIBN as an initiator. However, the number-average molecular weights (M_n 11 630−11 904 g/mol) of copolymerized products based on ethylene-linked complexes **1**−**3** are slightly larger than those (M_n 8130−9229 g/mol) from phenylene-linked complexes **4**−**6** on the same copolymerization conditions, indicating the presence of a small difference in reactivity among the two series of complex monomers. Moreover, as to three different copolymerizations carried out with MMA to complex **2** ratios of 50:1, 100:1, and 200:1, an almost linear relationship between the molecular weight (M_n) versus MMA to complex **2** molar ratio suggests a random distribution of MMA along the polymer backbone.

PXRD patterns of **[Zn(L″)(Py)Nd(NO$_3$)$_3$]**-containing doped and copolymerized PMMA hybrid materials (Supporting Information, Figure S5) show only amorphous peaks of pure PMMA, suggesting that in each of the hybrid materials, the heterobinuclear complex molecule is homogeneously distributed in the PMMA matrix and that the crystalline peaks of the complex are not detected due to the lower concentration. Moreover, TG analysis of the two kinds of PMMA-supported hybrid materials shows a slight increase of 21 °C for the T_{onset} in comparison with the pure PMMA (Supporting Information, Figure S6), and the decomposition with maxima around the higher temperature interval (394−400 °C) than that (290−307 °C) of complexes **2** and **5**, which suggests that the thermal stabilities of two kinds of PMMA-supported hybrid materials are essentially improved by doping or copolymerization. Furthermore, the XPS data are used to determine the representative **[Zn(L″)(Py)Ln(NO$_3$)$_3$]**-containing (Ln = Nd or Gd) doped or copolymerized hybrid material composition and metal coordination environment (Figure 5), in which the Zn^{2+} $^2p_{3/2}$ and $^2p_{1/2}$

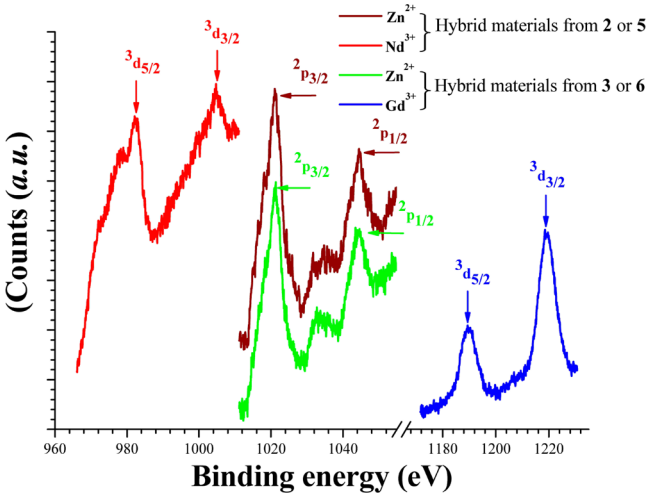

Figure 5. Representative XPS data of two series of hybrid materials **PMMA/[Zn(L″)(Py)Ln(NO$_3$)$_3$]** and **Poly(MMA-*co*-[Zn(L″)(Py)Ln(NO$_3$)$_3$])** (**L″** = **L^1** or **L^2**; Ln = Nd or Gd).

peaks at 1021.1 and 1044.4 eV and the Ln^{3+} (Ln = Nd or Gd) $^3d_{5/2}$ and $^3d_{3/2}$ peaks corresponding well to the expected binding energy values for Ln^{3+} bound to oxygen at 982.2 and 1004.9 eV, 1189.5 and 1219.3 eV, respectively,[35] are observed. The further quantitative XPS analyses reveal that the definite molar ratio of 1:1 of Zn^{2+} and Ln^{3+} in the two kinds of hybrid materials is observed, and the metal contents of 1.7 mol % for doping and 1.3 mol % for copolymerization are 60−81% of the theoretical values with the feed molar ratio of 100:1, while they are well in accordance with the ^{1}H NMR analysis results of their corresponding **[Zn(L″)(Py)La(NO$_3$)$_3$]**-containing hybrid materials.

3.4. Photophysical Properties of [Zn(L″)(Py)Ln(NO$_3$)$_3$], Doped Hybrid Materials PMMA/[Zn(L″)(Py)Ln(NO$_3$)$_3$], and Copolymerized Hybrid Materails Poly(MMA-*co*-[Zn(L″)(Py)Ln(NO$_3$)$_3$]) in Solid State. For complexes **[Zn(L″)(Py)Ln(NO$_3$)$_3$]** (Ln = Nd or Gd; n = 1 or 2), the doped hybrid materials **PMMA/[Zn(L″)(Py)Ln(NO$_3$)$_3$]**, and copolymerized hybrid materails **Poly(MMA-*co*-[Zn(L″)(Py)Ln(NO$_3$)$_3$])**, their photophysical properties in solid state at room temperature or 77 K were examined and also summarized in Table 2, Figures 6−9, and Supporting Information, Figures S7−13. As shown in Figure 6, the diffuse reflectance (DR) spectra of the PMMA-supported doped hybrid materials from **2**−**3** and **5**−**6** exhibit two relatively broader absorption bands than those of complexes **2**−**3** and **5**−**6** (Supporting Information, Figure S7), where one in the UV region can be assigned to electronic transitions from the organic moieties of PMMA and coordinated Schiff-base ligands, and the other in the visible to NIR region is attributed to the

dx.doi.org/10.1021/ic500132n | Inorg. Chem. 2014, 53, 5950−5960

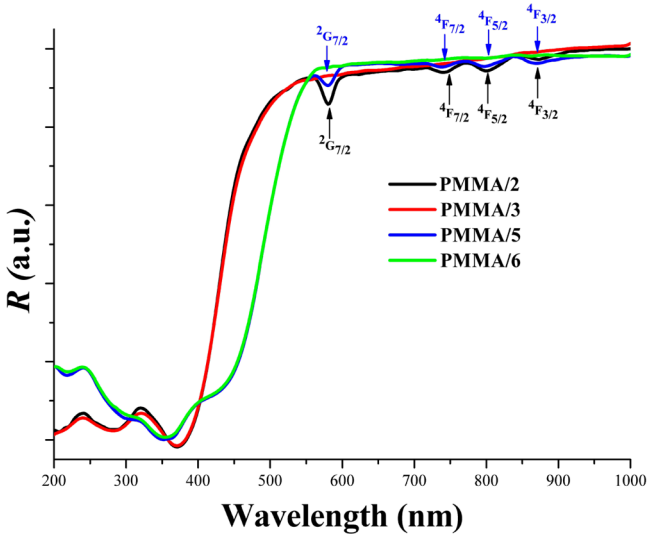

Figure 6. DR spectra of **PMMA/2**, **PMMA/3**, **PMMA/5**, and **PMMA/6** from the monomer feeding molar ratio of 100:1 in solid state at room temperature.

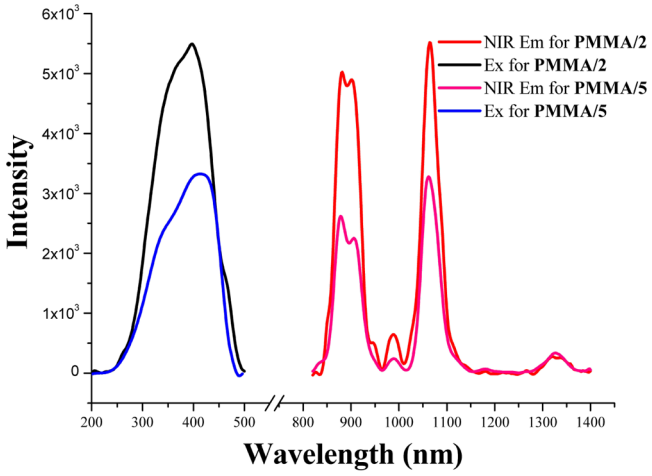

Figure 7. NIR emission and excitation spectra of doped hybrid materials **PMMA/2** and **PMMA/5** from the monomer feeding molar ratio of 100:1 in solid state at room temperature.

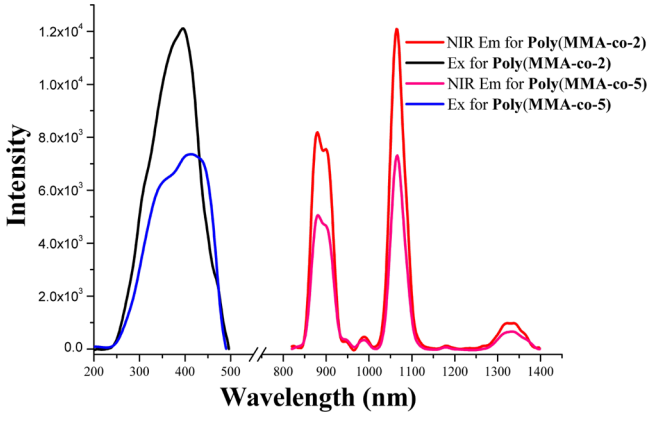

Figure 8. NIR emission and excitation spectra of copolymerized hybrid materials **Poly(MMA-*co*-2)** and **Poly(MMA-*co*-5)** from the monomer feeding molar ratio of 100:1 in solid state at room temperature.

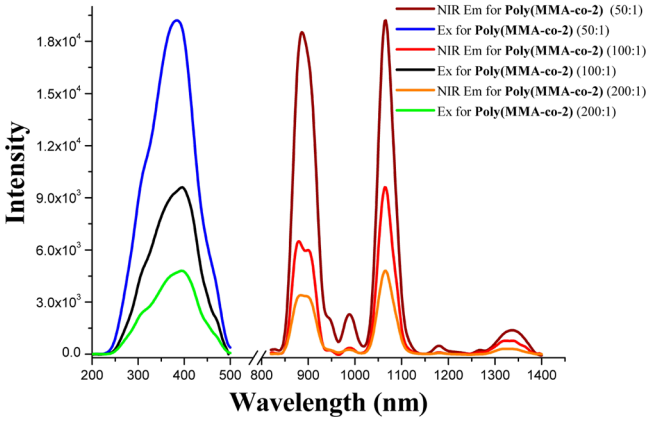

Figure 9. NIR emission and excitation spectra of copolymerized hybrid materials **Poly(MMA-*co*-2)** from different monomer feeding molar ratios (50:1, 100:1, or 200:1) in solid state at room temperature.

characteristic transitions levels of the corresponding Nd^{3+} ion from the ground level $^2G_{7/2}$, $^4F_{7/2}$, $^4F_{5/2}$, or $^4F_{3/2}$ to the higher energy levels. Because of the characteristic absorption bands of Gd^{3+} ion commonly appearing above 1000 nm, they are not discerned in the corresponding samples. Upon excitation of the chromophore's absorption band (λ_{ex} = 398 nm for **PMMA/2** or λ_{ex} = 418 nm for **PMMA/5**), for both **PMMA/2** and **PMMA/5** in solid state, the weak visible emissions and the similar characteristic NIR emissions of the Nd^{3+} ion ($^4F_{3/2} \rightarrow {}^4I_{J/2}$, J = 9, 11, 13; shown in Figure 7) to those of the complex **2** or **5** in both solution (Figure 4) and solid state (Supporting Information, Figure S8) are observed. Unlike the observed NIR emissions of complex **2** or **5** and doped hybrid materials from **2** or **5**, both complexes **3** and **6** and the doped hybrid materials from **3** and **6** just display the typical visible emissions, as shown in Supporting Information, Figures S9−10, respectively. It is worth noting that the maximum excitation positions (λ_{ex} = 398 or 418 nm) of the spectra for the doped hybrid materials are both red-shifted as compared to the solution or solid spectra of complexes **2** and **5**, which can be attributed to the enhanced light absorption of the PMMA matrix.[36] On the basis of the typical time-resolved luminescent experiment for NIR luminescent **PMMA/2** or **PMMA/5**, their luminescent decay curves can also be fitted monoexponentially with lifetime of 2.72 or 1.65 μs, respectively. These values, together with the calculated intrinsic quantum yields (1.09% or 0.66%), are almost in accordance with those found for complex **2** or **5** in solution and solid, showing that the host PMMA matrix does not interact with the complex and has no influence on the sensitization process of the Nd^{3+} ion.[37] Although the luminescence intensity of the Nd^{3+} emissions increase with increasing Nd^{3+} content for **PMMA/2**, as shown in Supporting Information, Figure 11S, the concentration self-quenching effect begins at a doped monomer feeding molar ratio of 50:1.

As to the copolymerized hybrid materials based on complexes **2**, **3**, **5**, and **6**, as shown in Supporting Information, Figures S12 and S13, besides the similar broad absorption in the visible to NIR region assigned to the characteristic transition levels of the corresponding Ln^{3+} ion, a relatively broader absorption band in the UV region than those of the PMMA-supported doped hybrid materials is observed from their DR spectra in solid state. This should be due to the increased molecular conjugation for the metallopolymers.[38] Photoexcitation of the corresponding chromophore in the rigion of 220−510 nm (λ_{ex} = 396 nm for

dx.doi.org/10.1021/ic500132n | *Inorg. Chem.* 2014, 53, 5950−5960

Poly(MMA-*co*-2) or λ_{ex} = 412 nm for **Poly(MMA-*co*-5)** also gives rise to characteristic ligand-field splitting emissions of the Nd^{3+} ($^4F_{3/2} \rightarrow {}^4I_{J/2}$, J = 9, 11, 13; shown in Figure 8) in the NIR region, while the residual visible emissions, especially from complex **2**, are almost completely quenched. These results, together with the similar red shift of the maximum excitation positions, suggest that more efficient energy transfer of the two extended metallopolymers takes place from a localized excited state.[39] The typical luminescent decay curves for the excited Nd^{3+} ion at the $^4F_{3/2}$ state in the two metallopolymers are also fitted well by a single-exponential function in agreement with those of the complexes and the doped hybrid materials. However, the slight increase of lifetimes (3.01 μs for **Poly(MMA-*co*-2)** and 1.89 μs for **Poly(MMA-*co*-5)**) of the two NIR luminescent metallopolymers, after being grafted into the PMMA matrix, increases the intrinsic quantum yield (1.21% or 0.76%) of the Nd^{3+} emission more than that of the corresponding complex (1.10−1.12% or 0.65−0.67%) or the corresponding hybrid material in solid state (1.09% or 0.66%), which should be due to the molecular extension of the two metallopolymers.[40] From the viewpoint of energy level's match, the extension gives the smaller energy gap (ΔE^3 = 6380 cm^{-1} or ΔE^1 = 7092 cm^{-1}) between the excited state of the chromorphore to the Nd^{3+} ion excitied state ($^4F_{3/2}$) than that in corresponding complex or corresponding doped hybrid materials, resulting in the lower nonradiative energy loss during the energy transfer. As to the relatively higher NIR insintric quantum yield of **Poly(MMA-*co*-2)** than that of **Poly(MMA-*co*-5)**, it should also be attributed to the combined ^{1}LC and ^{3}LC, while not only ^{1}LC for **Poly(MMA-*co*-5)**. Of particular note is to observe an almost linear relationship (shown in Figure 9) between the NIR emission intensity and concentration (50:1, 100:1, and 200:1) of complex **2** for **Poly(MMA-*co*-2)** metallopolymers, which shows the concentration self-quenching in Ln^{3+}-based doped hybrid materials[11] is prevented from the formation of uniform copolymerized hybrid materials even in solid state.

4. CONCLUSIONS

Two kinds of heterobinuclear Zn−Ln complexes $[Zn(L^n)(Py)Ln(NO_3)_3]$ (n = 1 or 2, Ln = La, Nd, or Gd), based on the divinylphenyl-modified Salen-type Schiff-base ligands with different linkers as the optical emitters, were introduced into the PMMA matrix to obtain PMMA-supported doped hybrid materials **PMMA/$[Zn(L^n)(Py)Ln(NO_3)_3]$** and Wolf Type II Zn^{2+}−Ln^{3+}-containing metallopolymers **Poly(MMA-*co*-$[Zn(L^n)(Py)Ln(NO_3)_3]$)**, respectively. The physically doped and controllable copolymerized hybrid materials from $[Zn(L^n)(Py)Nd(NO_3)_3]$ all show similar NIR luminescent properties compared with the complexes, while the grafted metallopolymer, especially from ethylene-linked Zn−Nd complex, endows the largest intrinsic quantum yield of the Nd^{3+} emission, and the concentration self-quenching of Nd^{3+}-based materials could be effectively prevented for the copolymerized hybrid materials in comparison with the doped hybrid materials. This result suggests that PMMA-supported Wolf Type II Zn^{2+}−Ln^{3+}-containing metallopolymers represent a new class of optical materials, which can be used in the pursuit of creating high color purity NIR polymer-based OLEDs.

■ ASSOCIATED CONTENT

Supporting Information

The synthesis and characterization of ligand H_2L^2, complexes **4**−**6**, doped hybrid materials **PMMA/$[Zn(L^2)(Py)Ln(NO_3)_3]$** (Ln = La, **4**; Ln = Nd, **5**; Ln = Gd, **6**), and copolymerized hybrid materials **Poly(MMA-*co*-$[Zn(L^2)(Py)Ln(NO_3)_3]$)** (Ln = La, **4**; Ln = Nd, **5**; Ln = Gd, **6**); selected bond lengths (Å) and angles (deg) for complexes **2**·H_2O·MeOH and **5**·0.5H_2O in Table S1; ^{1}H NMR spectra for H_2L^2, **4**, **PMMA/4**, and **Poly(MMA-*co*-4)** in $CDCl_3$ or DMSO-d_6−$CDCl_3$ (10:1 v/v) at room temperature; perspective drawing of the host heterobinuclear structure in **5**·0.5H_2O; visible emission and excitation spectra of H_2L^1, H_2L^2, and complexes **3** and **6** in absolute MeCN solution at 1×10^{-5} M at room temperature; schematic energy level diagram and energy transfer process of Nd^{3+} ion; PXRD patterns of PMMA, representative doped hybrid materials **PMMA/2** and **PMMA/5**, and representative copolymerized hybrid materials **Poly(MMA-*co*-2)** and **Poly(MMA-*co*-5)**; TG curves of **2** and **5**, PMMA, doped hybrid materials **PMMA/2** and **PMMA/5**, and copolymerized hybrid materials **Poly(MMA-*co*-2)** and **Poly(MMA-*co*-5)** from the monomer feeding molar ratio of 100:1; DR spectra of complexes **2**−**3** and **5**−**6** in solid state at room temperature; NIR and visible emission and excitation spectra of complexes **2**−**3** and **5**−**6** in solid state at room temperature; visible emission and excitation spectra of doped hybrid materials **PMMA/3** and **PMMA/6** with the monomer feeding molar ratio of 100:1 in solid state at room temperature; NIR emission and excitation spectra of doped hybrid materials **PMMA/2** from different monomer feeding molar ratios (50:1, 100:1, or 200:1) in solid state at room temperature; DR spectra of **Poly(MMA-*co*-2)**, **Poly(MMA-*co*-3)**, **Poly(MMA-*co*-5)**, and **Poly(MMA-*co*-6)** in solid state at room temperature; and visible emission and excitation spectra of copolymerized hybrid materials **Poly(MMA-*co*-3)** and **Poly(MMA-*co*-6)** in Figures S1−13, respectively. This material is available free of charge via the Internet at http://pubs.acs.org.

■ AUTHOR INFORMATION

Corresponding Author

*E-mail: lvxq@nwu.edu.cn. Phone: 86-29-88302312.

Notes

The authors declare no competing financial interest.

■ ACKNOWLEDGMENTS

This work is funded by the National Natural Science Foundation (21373160, 91222201, 21173165, 20871098), the Program for New Century Excellent Talents in University from the Ministry of Education of China (NCET-10-0936), the research fund for the Doctoral Program (20116101110003) of Higher Education, the Education Committee Foundation (11JK0588), the Science, Technology and Innovation Project (2012KTCQ01-37) of Shaanxi Province, Graduate Innovation and Creativity Fund (YZZ12038) of Northwest University, Hong Kong Research Grants Council (HKBU 202407 and FRG/06-07/II-16) in P. R. of China, the Robert A. Welch Foundation (Grant F-816), the Texas Higher Education Coordinating Board (ARP 003658-0010-2006), and the Petroleum Research Fund, administered by the American Chemical Society (47014-AC5).

■ REFERENCES

(1) (a) Kido, J.; Okamoto, Y. *Chem. Rev.* **2002**, *102*, 2357−2368. (b) Katkova, M. A.; Bochkarev, M. N. *Dalton Trans.* **2010**, 6599−6612.

(2) Bünzli, J.-C. G.; Eliseeva, S. V. *J. Rare Earths* **2010**, *28*, 824−842.
(3) Bünzli, J.-C. G.; Piguet, C. *Chem. Soc. Rev.* **2005**, *34*, 1048−1077.
(4) Bünzli, J.-C. G. *Chem. Rev.* **2010**, *110*, 2729−2755.
(5) Feng, J.; Zhang, H. J. *Chem. Soc. Rev.* **2013**, *42*, 387−410.
(6) Eliseeva, S. V.; Bünzli, J.-C. G. *Chem. Soc. Rev.* **2010**, *39*, 189−227.
(7) (a) Ward, M. D. *Coord. Chem. Rev.* **2007**, *251*, 1663−1677. (b) Ward, M. D. *Coord. Chem. Rev.* **2010**, *254*, 2634−2642.
(8) Chen, F. F.; Chen, Z. Q.; Bian, Z. Q.; Huang, C. H. *Coord. Chem. Rev.* **2010**, *254*, 991−1010.
(9) Comby, S.; Bünzli, J.-C. G. Lanthanide Near-Infrared Luminescence in Molecular Probes and Devices. In *Handbook on the Physics and Chemistry of Rare Earths;* Gneidner, K. A., Jr., Bünzli; J.-C. G., Pecharsky, V. K., Eds.; Elsevier Science B.V.: Amsterdam, The Netherlands, 2007; Vol. *37*, pp 217−470.
(10) Bünzli, J.-C. G.; Eliseeva,S. V. *Springer Series on Fluorescence, Vol. 7, Lanthanide Spectroscopy, Materials, and Bio-applications;* Hänninen, P., Härmä, H., Eds.; Springer Verlag: Berlin, Germany, 2010; Vol. *7*, ch. 2.
(11) Carlos, L. D.; Ferreira, R. A. S; Bermudez, V. de Z.; Julian-Lopez, B.; Escribano, P. *Chem. Soc. Rev.* **2011**, *40*, 536−549.
(12) (a) Binnemeans, K. *Chem. Rev.* **2009**, *109*, 4284374. (b) Sanchez, C.; Belleville, P.; Popallad, M.; Nicole, L. *Chem. Soc. Rev.* **2011**, *40*, 696−753. (c) Yan, B. *RSC Adv.* **2012**, *2*, 9304−9324.
(13) Stanley, J. M.; Holliday, B. J. *Coord. Chem. Rev.* **2012**, *256*, 1520−1530.
(14) Wolf, M. O. *Adv. Mater.* **2001**, *13*, 545−553.
(15) (a) Wong, W.-Y. *Dalton Trans.* **2007**, 4495−4510. (b) Wong, W.-Y.; Harvey, P. D. *Macromol. Rapid Commun.* **2010**, *31*, 671−713. (c) Wong, W.-Y.; Ho, C.-L. *Acc. Chem. Res.* **2010**, *43*, 1246−1256. (d) Whittell, G. R.; Hager, M. D.; Schubert, U. S.; Manners, I. *Nat. Mater.* **2011**, *10*, 176−188. (e) Ho, C.-L.; Wong, W.-Y. *Coord. Chem. Rev.* **2011**, *255*, 2469−2502. (f) Ho, C.-L.; Wong, W.-Y. *Coord. Chem. Rev.* **2013**, *257*, 1614−1649.
(16) (a) Pei, J.; Liu, X. L.; Yu, W. L.; Lai, Y. H.; Liu, Y. H.; Cao, R. *Macromolecules* **2002**, *35*, 7274−7280. (b) Balamurugan, A.; Reddy, M. L. P.; Jayakannan, M. *J. Phys. Chem. B* **2009**, *113*, 14128−14138.
(17) Meyers, A.; Kimyonok, A.; Weck, M. *Macromolecules* **2005**, *38*, 8671−8678.
(18) (a) Ling, Q.; Song, Y.; Ding, S. J.; Zhu, C.; Chan, D. S. H.; Kwong, D.-L.; Kang, E.-T.; Neoh, K.-G. *Adv. Mater.* **2005**, *17*, 455−459. (b) Xu, H.; Zhu, R.; Zhao, P.; Huang, W. *J. Phys. Chem. C* **2011**, *115*, 15627−15638.
(19) Chen, X. Y.; Yang, X. P.; Holliday, B. J. *J. Am. Chem. Soc.* **2008**, *130*, 1546−1547.
(20) Li, J. F.; Song, F. Y.; Wang, L.; Jiao, J. M.; Cheng, Y. X.; Zhu, C. J. *Macromol. Rapid Commun.* **2012**, *33*, 1268−1272.
(21) (a) Lo, W.-K.; Wong, W.-K.; Wong, W.-Y.; Guo, J. P.; Yeung, K.-T.; Cheng, Y.-K.; Yang, X. P.; Jones, R. A. *Inorg. Chem.* **2006**, *45*, 9315−9325. (b) Bi, W. Y.; Lü, X. Q.; Chai, W. L.; Song, J. R.; Wong, W.-K.; Yang, X. P.; Jones, R. A. *Z. Anorg. Allg. Chem.* **2008**, *634*, 1795−1780. (c) Pasatoiu, T. D.; Tiseanu, C.; Madalan, A. M.; Jurca, B.; Duhayon, C.; Sutter, J. P.; Andruh, M. *Inorg. Chem.* **2011**, *50*, 5879−5889.
(22) (a) Bi, W. Y.; Wei, T.; Lü, X. Q.; Hui, Y. N.; Song, J. R.; Zhao, S. S.; Wong, W.-K.; Jones, R. A. *New J. Chem.* **2009**, *33*, 2326−2334. (b) Wang, H. L.; Zhao, D. P.; Ni, Z. H.; Li, X. Y.; Tian, L. J.; Jiang, J. Z. *Inorg. Chem.* **2009**, *48*, 5946−5956.
(23) (a) Lü, X. Q.; Bi, W. Y.; Chai, W. L.; Song, J. R.; Meng, J. X.; Wong, W.-Y.; Wong, W.-K.; Jones, R. A. *New J. Chem.* **2008**, *32*, 127−131. (b) Lü, X. Q.; Feng, W. X.; Hui, Y. N.; Wei, T.; Song, J. R.; Zhao, S. S.; Wong, W.-Y.; Wong, W.-K.; Jones, R. A. *Eur. J. Inorg. Chem.* **2010**, 2714−2722.
(24) Burrow, C. E.; Burchell, T. J.; Lin, P.-H.; Habib, F.; Wernsdorfer, W.; Clérac, R.; Murugesu, M. *Inorg. Chem.* **2009**, *48*, 8051−8053.
(25) (a) Yang, X. P.; Jones, R. A.; Wong, W.-K.; Oye, M. M.; Holmes, A. L. *Chem. Commun.* **2006**, 1836−1838. (b) Lü, X. Q.; Bi, W. Y.; Chai, W. L.; Song, J. R.; Meng, J. X.; Wong, W.-Y.; Wong, W.-K.; Yang, X. P.; Jones, R. A. *Polyhedron* **2009**, *28*, 27−32.
(26) Coulson, D. R.; Satek, L. C.; Grim, S. O. *Inorg. Synth.* **2007**, *13*, 121−124.
(27) Sheldrick, G. M. *SHELXL-97,* Program for crystal structure refinement; University of Göttingen: Göttingen, Germany, 1997.
(28) Sheldrick, G. M. *SADABS;* University of Göttingen: Göttingen, Germany, 1996.
(29) Braunecker, W. A.; Matyjaszewski, K. *Prog. Polym. Sci.* **2007**, *32*, 93−146.
(30) Ogasawara, K.; Watanabe, S.; Toyoshima, H.; Brik, M. G. *Handbook on the Physics and Chemistry of Rare Earths;* Gneidner, Jr., K. A., Bünzli, J.-C. G., Pecharsky, V. K., Eds.; Elsevier Science B.V.: Amsterdam, The Netherlands, 2007; Vol. *37*, p 231.
(31) Weber, M. J. *Phys. Rev.* **1968**, *171*, 283−291.
(32) Carnall, W. T.; Fields, P. R.; Rajnak, K. *J. Chem. Phys.* **1968**, *49*, 4443−4446.
(33) Dexter, D. L. *J. Chem. Phys.* **1953**, *21*, 836−850.
(34) (a) Lunstroot, K.; Driesen, K.; Nockemann, P.; Viau, L.; Mutin, P. H.; Viouxb, A.; Binnemans, L. *Phys. Chem. Chem. Phys.* **2010**, *12*, 1879−1885. (b) Fan, W. Q.; Feng, J.; Song, S. Y.; Lei, Y. Q.; Zheng, G. L.; Zhang, H. J. *Chem.—Eur. J.* **2010**, *16*, 1903−1910. (c) Biju, S.; Eom, Y. K.; Bünzli, J.-C. G.; Kim, H. K. *J. Mater. Chem. C* **2013**, *1*, 6935−6944.
(35) Mercier, F.; Alliot, C.; Bion, L.; Thromat, N.; Toulhoat, P. *J. Electron Spectrosc. Relat. Phenom.* **2006**, *150*, 21−26.
(36) Raj, D. B. A.; Francis, B.; Reddy, M. L. P.; Butorac, R. R.; Lynch, V. M.; Cowley, A. H. *Inorg. Chem.* **2010**, *49*, 9055−9063.
(37) Martín-Ramos, P.; Lavín, V.; Ramos Silva, M.; Martín, I. R.; Lahoz, F.; Chamorro-Posada, P.; Paixão, J. A.; Martín-Gil, J. *J. Mater. Chem. C* **2013**, *1*, 5701−5710.
(38) Sun, L. N.; Zhang, H. J.; Yu, J. B.; Yu, S. Y.; Peng, C. Y.; Dang, S.; Guo, X. M.; Feng, J. *Langmuir* **2008**, *24*, 5500−5507.
(39) Fan, W. Q.; Feng, J.; Song, S. Y.; Lei, Y. Q.; Zhou, L.; Zheng, G. L.; Dang, S.; Wang, S.; Zhang, H. J. *Nanoscale* **2010**, *2*, 2096−2103.
(40) Carlos, L. D.; Ferreiro, R. A. S.; Bermudez, V.; de, Z.; Ribeiro, S. J. L. *Adv. Mater.* **2009**, *21*, 509−534.